7-29-2019

Prognostics Models for Railroad Tapered Roller Bearings with Spall Defects on Inner or Outer Rings

Constantine Tarawneh
The University of Texas Rio Grande Valley

Jennifer Lima
The University of Texas Rio Grande Valley

Nancy De Los Santos
The University of Texas Rio Grande Valley

Robert Jones
The University of Texas Rio Grande Valley

Recommended Citation

Constantine Tarawneh, Jennifer D. Lima, Nancy De Los Santos & Robert E. Jones (2019) Prognostics Models for Railroad Tapered Roller Bearings with Spall Defects on Inner or Outer Rings, Tribology Transactions, 62:5, 897-906, DOI: 10.1080/10402004.2019.1634228

Prognostics Models for Railroad Tapered-Roller Bearings with Spall Defects on Inner or Outer Rings

Constantine Tarawneh, Ph.D., first author[1]
Mechanical Engineering Department
University of Texas Rio Grande Valley (UTRGV)
University Transportation Center for Railway Safety (UTCRS)
1201 W. University Dr., Edinburg, TX 78539
constantine.tarawneh@utrgv.edu
https://orcid.org/0000-0002-4074-5627

Jennifer D. Lima, second author
Mechanical Engineering Department, UTRGV
University Transportation Center for Railway Safety (UTCRS)
jennifer.lima01@utrgv.edu

Nancy De Los Santos, third author
Mechanical Engineering Department, UTRGV
University Transportation Center for Railway Safety (UTCRS)
nancy.delossantos01@utrgv.edu

Robert E. Jones, Ph.D., fourth author
Mechanical Engineering Department, UTRGV
University Transportation Center for Railway Safety (UTCRS)
robert.jones@utrgv.edu

[1] Corresponding author, contact phone (956) 665-2607 or (956) 665-3510.

Prognostics Models for Railroad Tapered-Roller Bearings with Spall Defects on Inner or Outer Rings

ABSTRACT

Rolling contact fatigue (RCF) is one of the major causes of failure in railroad bearings used in freight service. Subsurface inclusions resulting from impurities in the steel used to fabricate the bearings initiate subsurface fatigue cracks which propagate upwards and cause spalling of the rolling surfaces. These spalls start small and propagate as continued operation induces additional crack formation and spalling. Studies have shown that the bearing temperature is not a good indicator of spall initiation. In many instances, the temperature of the bearing increases markedly only when the spall has spread across major portions of the raceway. In contrast, vibration signatures can be used to accurately detect spall initiation within a bearing and can track spall deterioration. No monitoring technique can indicate the growth rate of a spall nor determine residual useful life. Hence, the main objective of this study is to develop reliable prognostic models for spall growth within railroad bearings that are based on actual service life testing rather than theoretical simulations. The data used to devise the models presented here has been acquired from laboratory and field testing that started in 2010. Growth models are provided for spalls initiating on the bearing inner (cone) and outer (cup) rings. Coupling these prognostic models with a previously developed vibration-based bearing condition-monitoring algorithm will provide the rail industry with an efficient tool that can be used to plan

proactive maintenance schedules that will mitigate unnecessary and costly train stoppages and delays and will prevent catastrophic derailments.

Keywords: spall growth models, spall propagation, proactive maintenance, bearing defect growth trends, bearing condition monitoring

INTRODUCTION AND BACKGROUND

The heavy loads carried by a freight railcar are distributed equally among eight tapered-roller bearings that sit at the ends of the wheel-axle assemblies. A typical tapered-roller bearing, shown in Fig. 1, has one outer ring (cup) and two inner rings (cones) with rollers transferring the load between the cup and the cones. The bearing outer ring (cup) is supported on one side by the side-frame of the truck/bogie. Hence, the load path travels from the railcar side frame to the bearing cup through the bearing adapter and from the cup to the cones through the rollers. The bearing cup is stationary and does not rotate unless it indexes slightly during service operation when the bearing is temporarily unloaded. The latter occurs when the railcar wheels hit a bump in the rail tracks causing the side-frame to briefly lose contact with the bearing adapter. Therefore, under normal bearing service operation, the top ‘hemisphere’ of the cup is always loaded and is referred to as the ‘loaded zone’, whereas, the bottom ‘hemisphere’ of the cup is referred to as the ‘unloaded zone’. The bearing inner rings (cones) are press-fit to the axle and rotate synchronously with the axle and wheels, undergoing cyclical loading and unloading as they rotate through the loaded and unloaded zones [2].

Rolling contact fatigue (RCF) which leads to spalling of the cup or cone raceways is one of the most common causes of railroad tapered-roller bearing failure [2-4]. According to Hertzian contact theory, maximum shear stresses are usually located 200-600 μm below the surface of rolling contact [2-4]. The presence of metallurgical impurities in this subsurface region can cause the local stress levels to reach values that exceed the endurance limit of the steel, which results in micro-cracks being initiated around these subsurface inclusions. With continued operation, the micro-cracks propagate until they reach the raceway surface causing parts of the metal to break off and creating what is known as a 'spall' [4-7]. The formation of spalls on bearing raceways is usually accompanied by metallic shards that are introduced to the bearing rolling components and lubricant. Debris pile-up can cause high pressure spikes as the bearing rollers continue to run along the inner and outer ring raceways, which causes further deterioration to these raceways [6]. Moreover, the shard pile-up in conjunction with the spalled raceway surfaces can trigger roller misalignment as the rollers enter the bearing loaded zone. Roller misalignment generally increases frictional heating as the rollers tend to slide against the rolling raceways rather than rotate normally. This results in higher bearing operating temperatures and premature lubricant breakdown [6-8]. Laboratory testing has demonstrated that continuing to operate the bearing after initial spalling has occurred will cause the bearing to degrade over time [8]. The study presented in this paper examines actual spall growth rates in bearing inner (cones) and outer (cups) rings that experienced spalling during field service and/or laboratory service-life testing.

It is important to note that empirically-based bearing prognostic models have not been well developed for rail service because of the highly stochastic nature of the bearing fatigue process and the great variability in service conditions. Bearings in rail service experience highly variable operating loads, speeds, temperature, and duty cycles. Although rolling contact fatigue (RCF) has been an active area of study by many researchers, the majority of the work has focused on ball and rolling element bearings or gears used for turbines or other machinery [3, 6, 7, 9-12] , and is not specific to railroad bearings. These studies mainly presented theoretical and analytical models that predict crack propagation and growth and contact fatigue life with minimal experimental validation or idealized geometry and loading. In contrast, the data collected for this study reflects nine years of laboratory testing under simulated service with varying speeds, loads, and bearing temperatures, as well as some field testing performed at the Transportation Technology Center, Inc. (TTCI) in 2015. The acquisition of new data is ongoing as the research team continues to track the spall defect growth in several bearing inner and outer rings. Li et al. [9] presented a dynamic prognostic prediction of defect propagation on rolling element bearings which modeled general rolling element bearings for machinery. Their model effectively described the growth of a symmetrically located, manufactured spall. The study presented here differs in that it is focused on freight railroad bearings with naturally generated and, therefore, randomly distributed original spalls. The stochastic nature of spall formation then translates into much greater scatter in observed spall growth behavior. Moreover, in this study, prediction of remaining useful life is derived from spall growth as a function of actual distance traveled under service operation conditions since that is the standard industry measure. This data represents a

significant population of spalls monitored over an extended period of operation with the ultimate goal being to establish, with a high degree of confidence, bounding rates of growth for spalls independent of spall location and operating speed, load, and temperature.

BEARING CLASS SELECTION FOR TESTING

There are four Association of American Railroad (AAR) bearing classes that are commonly used in the freight rail service in the U.S. and Canada. These four are classes F, K, E, and G tapered-roller bearings. The data for this study has been acquired from testing class F (6½"×12") and class K (6½"×9") tapered-roller bearings only since these two classes of bearings are interchangeable and are widely used in freight rail transport in the U.S. and Canada. Data provided by the two largest railroad bearing manufacturers in the U.S. indicates that class F and K bearings represent 90% of the entire bearing population used in freight rail followed by class E bearings with 6%, and class G with 4%. Since there are about 1.6 million freight cars in the U.S. and Canada and each freight car uses eight bearings, this translates to roughly 11.5 million class F and K bearings in use in our rail system. This statistic justifies the need to develop specific models for spall growth in these bearings.

Both class F and K bearings are fabricated out of AISI 8620 steel with the tapered-rollers being case-hardened. The dimensions of the main components of class F and K bearings are identical with the exception that the spacer ring width in a class K

bearing is 1.46 to 1.48 cm (0.575 to 0.5825 in), whereas, the spacer ring width in a class F bearing is 3.68 to 3.94 (1.45 to 1.55 in). The latter difference makes the width of the class K bearing outer ring (cup) about 2.34 cm (0.92 in) shorter than the corresponding class F bearing cup. Moreover, since the gap between the two cone (inner ring) assemblies is smaller in a class K bearing, the bearing manufacturer recommends that the two cone assemblies be properly lubricated but no grease be placed in the spacer region. Hence, the total amount of lubricating grease in a class K bearing is 0.3845 L (13 oz), whereas, a class F bearing has 0.6506 L (22 oz) of lubricating grease, of which, 0.2661 L (9 oz) is placed in the spacer region and 0.3845 L (13 oz) is used to lubricate the cone assemblies similar to what is done for a class K bearing. All other dimensions including all raceway profiles, number of rollers within the cage assembly, roller geometry, and inner ring (cone) geometry are identical for class F and K bearings. The bearings tested in this study all came from one manufacturer who supplies more than 75% of all freight railroad bearings sold in the U.S. and Canada.

Note that class K bearings were designed to replace class F bearings and have been doing so since 2001 yet there are many class F bearings still running in freight service today. For this reason, this study contains bearings from both classes. The authors have been involved in the testing and performance characterization of both classes of bearings since 2005 and have concluded that there are no discernable differences in the thermal and dynamic performances of these two bearing classes.

EXPERIMENTAL SETUP AND INSTRUMENTATION

The laboratory testing for this study utilized railroad bearing dynamic test rigs specifically designed to closely simulate field service. Two types of test rigs are available; one is a single railroad bearing rig pictured in Fig. 2, and the other is a four-bearing tester depicted in Fig. 3. Both test rigs can accommodate any Association of American Railroads (AAR) bearing class used for freight railcars in the U.S. and Canada. They are driven by a large 22.3 kW (30 hp) variable-speed motor that can provide rotational speeds that are equivalent to train operating speeds from 8 to 137 km/h (5 to 85 mph). Hydraulic cylinders were used to apply the vertical load to the test bearings in both testers. The hydraulic cylinder can apply maximum loads that are equivalent to 150% of the full-load of a class F or K bearing. Note that a 100% load (full-load) of a class F or K bearing corresponds to 153 kN (34.4 kips) as established by the AAR [13], whereas, an empty railcar load is approximately equivalent to 17% of the full-load or 26 kN (5.85 kips) for a class F or K bearing.

The single bearing tester (SBT) of Fig. 2 can apply vertical, lateral, and impact load to the bearing to mimic normal and abnormal bearing operation conditions. This tester can provide maximum lateral loads of up to 22 kN (5 kips) and maximum vertical loads of up to 222 kN (50 kips). Additionally, the tester can supply a variable frequency (0-3 Hz) impact load of up to 100g. To prevent overheating of the support bearings in the tester, a cooling circulation system was incorporated in which chilled water runs over the pillow blocks which house the support bearings. To simulate service conditions, the test

bearing was cooled using two industrial fans that provided an airflow of 23.4 km/h (14.5 mph) across the bearing cup. This tester is designed to facilitate the quick removal and mounting of the railroad bearing onto the test axle, on-site, without the need for the axle to be removed from the rig. This feature allows for faster and more frequent teardowns and inspections. This is why this tester was utilized to run bearings with spalls having areas greater than 6.45 cm^2 (1 in^2) for cones and 12.9 cm^2 (2 in^2) for cups as these larger spalls required more frequent measurement of the spall area due to more rapid spall growth.

The four-bearing test rig of Fig. 3 can accommodate four bearings pressed onto a test axle. This tester is specifically designed for long-duration service life testing of bearings where the bearings are run continuously at a prescribed load and speed for several months at a time. To simulate service conditions, test bearings are always placed in the middle two spots where the bearings are top-loaded as is the case in field service. The outer two bearings, which are bottom-loaded, are healthy bearings and are used as controls when testing spalled bearings. The four-bearing tester is enclosed in an environmental chamber that can produce ambient temperatures as low as -40°C (-40°F) and as high as 60°C (140°F). Airflow is directed over the bearings via two industrial fans at velocities comparable to those in the single bearing tester.

A data acquisition system (DAQ) was utilized to monitor and log the temperature and vibration signatures of the test bearings collected using K-type thermocouples and accelerometers, respectively. The temperature data were acquired at a sampling rate of

128 Hz once every 20 seconds, whereas, the vibration data was acquired at a sampling rate of 5120 Hz for four seconds at ten-minute intervals.

METHODOLOGY

The spall data used in this study came from two different sources; namely, service life testing of bearings with known subsurface inclusions on the bearing cone or cup [2, 4, 5, 14] and bearings that were removed from service and upon inspection were found to have a spall on either the cone or the cup [8]. In the case of the service life testing data, new healthy (defect-free) bearings were selected by the manufacturer and ultrasonically scanned to identify any subsurface inclusions within 600 μm of the rolling surfaces of the cones and cups [2, 4, 5]. These bearings were then run on the four-bearing tester pictured in Fig. 3 until they developed spall(s) during the service life test. Therefore, the distance traveled to initiate those spalls is known. For the bearings removed from commercial service due to spalling, the distance traveled leading to these spalls is unknown. However, it is important to note that these bearings did not seize in service and did not trigger either the thermal or acoustic wayside defect detection systems. These bearings were removed from field service because of defective wheels and upon teardown and inspection were found to have spall(s) less than 6.45 cm^2 (1 in^2) in total area on the inner (cone) or outer (cup) rings of the bearings. So, to ensure that both sets of data can be used in the analysis, the prognostic models developed in this study are not a function of the distance traveled leading to the spall initiation. Only distance traveled after the spall(s) have developed were considered in the results presented here.

A total of 23 bearings were used for this study. Of these, 20 were new bearings that were ultrasonically scanned by the manufacturer and were found to have subsurface inclusions on 11 outer rings (cups) and nine inner rings (cones). The remaining three bearings were removed from service and two were found to have cup spalls while the third had a cone spall. Though only 23 bearings were tested over the course of this study, many were run, removed for evaluation, then rerun repeatedly so that the growth of spalls could be tracked with distance traveled.

A typical service life test requires that new bearings are run for an equivalent distance of 402,325 km (250,000 mi). Two bearings can be tested simultaneously on the four-bearing tester and the duration of each service life test is about five months assuming no delays or interruptions in testing. To expedite testing and ensure worst-case operation conditions, both testers were run at 137 km/h (85 mph) and full-load (153 kN or 34.4 kips per bearing) for much of the testing period. Lower running speeds at an empty railcar load (17% of full-load) were utilized only briefly at the beginning of each test to allow the grease to break in and avoid sudden overheating of the bearings. Additionally, regions of the bearing outer ring (cup) that contain the worst subsurface inclusions, as indicated by the ultrasonic scanning, were oriented to place those defects top-center in the highest load region of the loaded zone [2]. For bearing cups that develop spalls, the region containing the spall is also placed top-center in the maximum load zone.

Testing typically commences on the four-bearing tester that can accommodate two top-loaded test bearings (middle two bearings). Bearings were run on this tester until they developed spalls with defect initiation detected by accelerometers. Once the spall area in a bearing reached 6.45 cm^2 (1 in^2) for cones or 12.9 cm^2 (2 in^2) for cups, the bearing was moved to the single bearing tester which allows for simpler and more frequent teardowns and inspections.

For over a decade now, the authors have been collecting vibration, load, and temperature histories from a wide range of healthy and defective bearings under various combinations of speed and load utilizing the two test rigs pictured in Fig. 2 and Fig. 3. A previous publication by the authors summarized the average operating temperatures of healthy and defective bearings for speeds ranging from 40 km/h (25 mph) to 137 km/h (85 mph) at loads simulating an empty railcar (17% of full-load) and a fully-loaded railcar (100% load corresponding to 153 kN or 34.4 kips per bearing) [15]. The defective bearings were mostly bearings containing spalls on the raceways of either the cones or cups. The temperature, load, and vibration data acquired from laboratory and field testing have been used to develop a bearing health-monitoring algorithm [16-17]. This algorithm has been shown to detect, with better than 95% confidence, spall initiation and propagation in the cone and cup raceways [16]. As validated by laboratory and field testing, the algorithm can detect spalls having an area as small as 0.645 cm^2 (0.1 in^2), can differentiate between spalls that develop on the cone raceways versus cup raceways, and can provide an estimate of the spall area to within 10% of the actual spall size.

The algorithm was utilized to track defect initiation and propagation within the test bearings. The bearings were pressed-off the test axle and disassembled based on one of two criteria: (1) anytime the bearing condition-monitoring algorithm indicated spall initiation and/or propagation, or (2) every 96,560 km (60,000 miles) of continuous un-interrupted operation. The second criterion was implemented to ensure that there were no spalls that developed undetected.

Upon disassembly, the bearings were carefully cleaned and subjected to a thorough visual inspection. To maintain a reliable record of any spall formation and/or progression while allowing rapid resumption of testing of the spalled bearing, a casting of the spall (defect) area was created with a low-melting, zero-shrinkage Bismuth alloy. The casting was done by enclosing the spall region using tacky tape with an upper use temperature of 204°C (400°F) to frame the area of interest. The molten Bismuth alloy, having a melting point of 80°C (176°F), was then poured into the frame, as demonstrated in Fig. 4. After the Bismuth hardened, it was removed, and the spall impression was painted to enhance the contrast of the defect against the rest of the molding. The casting was then photographed, and the digital image exported to an image preprocessor where a monochrome rendition of the image was created, as depicted in Fig. 5. This image was then analyzed using a commercial image processing package which measures spall area and other geometric parameters, as shown in Fig. 5. This spall area data is then compared to the corresponding vibration data in order to improve the accuracy of the bearing condition-monitoring algorithm used to estimate spall size and track growth.

Finally, during the 2015 field test performed at the Transportation Technology Center, Inc. (TTCI) in Pueblo, CO, four of the test bearings from this study, two having a cone spall and two having cup spalls, were mounted on a freight car and were run for about 161 km (100 mi) under various load, speed, and track conditions. This testing was carried out to validate the efficacy of the bearing condition-monitoring algorithm in identifying cone and cup spalls and tracking their deterioration [16]. The field test showed no discernable difference between the performance profile of the bearings whether loaded in the laboratory testers or in the field. These field-tested bearings were returned to the laboratory where testing resumed in the single bearing rig.

RESULTS AND DISCUSSION

Bearing Inner Rings (Cones)

The cone spall area plotted against the total distance traveled since spalling is presented in Fig. 6. Total distance traveled refers to the absolute distance the bearing ran, encompassing both loaded (full-load) and unloaded (empty railcar) operation conditions. The data points were separated into two categories; spalls with areas above 6.45 cm^2 (1 in^2) and spall areas below 6.45 cm^2. A horizontal line was plotted in Fig. 6 at the 6.45 cm^2 (1 in^2) tick mark, and different data markers were used to differentiate between the two categories. From the figure, the cone spall area grows linearly ($R^2 = 0.86$) with distance traveled for spall sizes above 6.45 cm^2, whereas, for cone spall areas below 6.45 cm^2, the data is more scattered as indicated by the lower coefficient of determination ($R^2 = 0.38$) for the linear correlation. One explanation for these trends is that cone spalls

larger than 6.45 cm^2 (1 in^2) usually span the entire width of the cone raceway, as seen in Fig. 4; hence, their growth is less random and correlates better with total distance traveled during operation.

The spall area growth ratio is defined as the ratio of the current spall area to the original spall area at initiation. The cone spall area growth ratio as a function of total distance traveled, plotted in Fig. 7, shows behavior similar to Fig. 6, with two different trends showing for the two size regimes. The two trends are associated with cone spalls either above or below 6.45 cm^2 (1 in^2). The linear correlation labeled y_1 describes the trend for the spalls with areas above 6.45 cm^2, while the linear correlation y_2 describes the trend for spall areas below 6.45 cm^2. From Fig. 7, it can be observed that the slope in the correlation for cone spall areas above 6.45 cm^2 is steeper than for areas below 6.45 cm^2. This implies that there is a fundamental change in the growth pattern above a spall area of 6.45 cm^2, so that spall growth accelerates. One partial explanation for this is that tapered-roller bearing spalls will typically grow along the width (perpendicular to roll direction) of the rolling raceway until they reach the edges. Once a spall has bridged the entire raceway, it propagates circumferentially along the raceway. Without the un-spalled shoulders, the roller penetration into the spalled area will increase. This growth pattern can be observed in both inner (cone) and outer (cup) rings as depicted in Fig. 8 and Fig. 9, respectively. Another explanation for the faster propagation of spalls above the 6.45 cm^2 threshold is that as the spall area increases, the sliding friction will increase, inducing increased vibration and yielding faster degradation [7].

The average spall area growth rate is defined as the difference in area between the current spall size and the original spall size divided by the total distance traveled since the spall first formed. An instantaneous spall area growth rate is found by dividing the change in spall area between two consecutive instances by the distance traveled between these two instances. The average growth rate was chosen instead of the instantaneous growth rate for two main reasons; (1) the main objective of model development is to predict the average remaining useful life of bearings in terms of travel distance after they initiate a spall, and (2) the intervals between inspections and the growth steps of spalls vary randomly which results in significant variation in instantaneous spall area growth rates. Using average rates smooths out the effects of this variation.

The average cone spall area growth rate in [cm^2/km] as a function of total distance traveled is given in Fig. 10. Again, two trends emerge for cone spall sizes above or below 6.45 cm^2 (1 in^2). Both trends indicate an exponential decay with relatively high R^2 values, which suggests that the initial growth rate for each stage is high and exponentially decreases with distance traveled.

Table 1 provides the cone spall area growth rate maximum, minimum, and average values. These values were split into two categories; cone spall areas less than or greater than 6.45 cm^2 (1 in^2). The average growth rate values for cone spalls given in Table 1 support the earlier findings that cone spall sizes greater than 6.45 cm^2 (1 in^2) grow at a faster rate than cone spalls with areas less than 6.45 cm^2. When coupled with a spall detection system, the results displayed in Fig. 10 and Table 1 suggest that it is

possible to rapidly determine a date or distance for future removal of spalled bearings that does not disrupt operations and without adversely affecting system reliability. Hence, immediate stoppage and the resulting cost and system disruption is avoided.

For example, considering the maximum growth rate of 1.28×10^{-4} cm^2/km, it would take about 1,090,000 km (677,300 mi) of operation for an average initial cone spall to grow to 50% of the cone raceway surface area. Note that, for a class F or K bearing, the cone raceway surface area is about 279 cm^2 (43 in^2), whereas, the cup raceway area is about 367 cm^2 (57 in^2) per raceway. Even allowing for much more conservative estimates, railcar owners will have an adequate operational window to plan for a wheel-set replacement with minimal disruption to operation while maintaining maximum system reliability.

Bearing Outer Rings (Cups)

The cup spall area versus total distance traveled during operation is presented in Fig. 11. The data exhibits similar behavior to that of Fig. 6 for cone spalls, but the threshold between the two growth regimes seems to be at the 12.9 cm^2 (2 in^2) spall area. Two linear correlations represent the data shown in Fig. 11, one for cup spall areas above 12.9 cm^2 with a coefficient of determination (R^2) value of 0.81, and a second for cup spall areas below 12.9 cm^2 with an R^2 value of 0.34. As was the case for the cones, the slopes of the two linear correlations seen in Fig. 11 suggest a faster growth rate for spall areas above 12.9 cm^2. Again, once the spall spreads across the width of the raceway, it

will start growing along the circumference of the raceway, as demonstrated in Fig. 8 and Fig. 9.

Note that the threshold areas of 12.9 cm^2 (2 in^2) for the outer rings (cups) and 6.45 cm^2 (1 in^2) for the inner rings (cones) are empirical and were noticed when the results were plotted. The authors offer the following hypothesis for these thresholds. Referring to Fig. 12, it can be seen that the projected area of a tapered-roller on the cup raceway is about 11.68 cm^2 (1.81 in^2). Since the spall perimeter is highly variable, it is likely that a spall area approaching the projected area of the roller is necessary to permit the roller to completely enter the defect depression and engage the spall shoulder with a substantial lateral load rather than a predominately vertical contact pressure. This will result in increased subsurface shear stress below the shoulder and, thus, an increased rate of growth. The 50% smaller area threshold observed for cone spalls is probably due to the convex surface of the cone which permits rollers to achieve significant lateral engagement with the shoulder of the spall at a smaller defect area while it simultaneously results in about 10% higher subsurface Hertzian shear stress. In addition, though the cone rotates so that a spall spends part of its time outside of the loaded zone, every point on the cone will pass through the most heavily-loaded point on the bearing every cycle.

Spall initiation, on average, takes longer to occur than propagation. Once the spall forms as a small pit (~0.645 cm^2 or 0.1 in^2 in area), propagation rate will increase continuously. In general, spalls in both cups and cones spread across the width of the raceways first before starting to grow along the raceway circumference. Hence, as the

spall reaches a certain size, the spall propagation will hasten markedly with total distance traveled during operation. This latter trend is apparent in Fig. 13 which gives the cup spall growth ratio as a function of total distance traveled. Looking at Fig. 13, it can be observed that the cup spall growth ratio increases exponentially after 160,000 km (~100,000 mi) of operation. Note that the circled data point in Fig. 13 and Fig. 14 is an outlier and was not used to formulate the correlations provided in the figures. The associated bearing was uncharacteristically poor-quality steel that contained many subsurface inclusions and impurities. This bearing was produced during the manufacturer's trial run to certify a new steel supplier, which resulted in the manufacturer not qualifying this supplier.

Figure 14 gives the cup spall area growth rate in [cm^2/km] as a function of total distance traveled since initiation. As previously explained, spall growth is largely affected by the raceway boundaries. From Fig. 14, it can be seen that the cup spall area growth rate is initially high as the spall initiates and propagates fast, but it starts to slow down as the spall reaches the raceway boundaries. The latter behavior is exhibited by the y_2 growth rate relation of Fig. 14 for cup spalls with areas less than 12.9 cm^2. With continued operation, once the spall has spread across the width of the raceway, the cup spall area growth rate increases noticeably as the spall starts to grow along the circumference of the raceway unhindered but slows down as the cup spall area moves away from the region of full-load application. The latter is demonstrated by y_1 growth rate relation of Fig. 14 for cup spalls with areas greater than 12.9 cm^2.

Table 1 also lists the cup spall area growth rate maximum, minimum, and average values. The values are larger for spall sizes greater than 12.9 cm^2 (2 in^2). But more importantly, when comparing the values for cones to those for cups, it is apparent that cup spalls will grow significantly faster. Since the contact stresses between a roller and cone are approximately 20% higher than for a roller against the cup, it is unlikely the rate difference is due to differences in the contact stress. The difference in rate is probably due to the mode of bearing operation in rail service. While the bearing cup remains stationary, the cones rotate in unison with the axle and wheels, undergoing cyclic loading and unloading as they enter and exit the loaded and unloaded regions of the bearing. In this study, the cup spalls were placed directly under the applied load in the loaded zone, so they were never unloaded during bearing operation. This represents a worst-case loading for a cup spall and cannot occur for the rotating cone spalls. Hence, each cup spall sees many more roller impacts per kilometer of operation than a spall on the rotating cone will experience.

Finally, as in the example for cone spalls, if we assume the maximum growth rate of 6.52×10^{-4} cm^2/km with a starting spall of negligible size, it would still take 281,000 km (175,000 mi) of operation for a cup spall to grow to 50% of the cup raceway surface area (367 cm^2 or 57 in^2). Therefore, for both cone and cup spalls, the railcar operators have enough time to schedule a convenient maintenance stop without having to halt the train mid-route causing unnecessary and costly delays to rail operations.

CONCLUSIONS

This study and its findings represent work which started in 2010 and is still ongoing as tracking of spall propagation resumes. In previous publications [18, 19], the authors presented initial data and preliminary models for cone and cup spalls separately. The current paper presents refined models based on a larger dataset for cone and cup spall growth as a function of distance traveled.

Several conclusions can be drawn from the data. First, spall size affects growth rates in both bearing cups and cones. In both cases, it has been generally observed that once a spall initiates on the cone or cup raceway, it will grow and spread across the width of the raceway until the boundaries are reached. After that, the spall will continue to propagate with distance traveled during operation and will grow along the circumference of the raceway. This study identifies threshold spall areas where the growth rate transitions from lower to higher rates. These thresholds are approximately 6.45 cm^2 (1 in^2) for cone spalls, and 12.9 cm^2 (2 in^2) for cup spalls. These areas are likely related to the contact surface areas at full-load conditions between the roller and cone and cup. Spalls larger than these sizes will consistently permit the roller to fully enter the spall depression and interact with the shoulders of the spall with a larger lateral component which has a greater effect on subsurface shear and, thus, spall growth rate.

From the average spall area growth rate results presented, it is apparent that spalls will grow at a markedly faster rate in bearing cups as compared to bearing cones. The

latter finding is partly explained by the fact that cups are generally stationary and so will be loaded continuously if in the load zone, whereas, cones rotate with the axle and so a spall will enter and exit the loaded region of the bearing. Hence, in any field application, it will be important to identify whether the spall has initiated on the bearing cup (outer ring) or the cone (inner ring) to accurately predict the spall growth trend. The bearing condition-monitoring algorithm developed by the authors can reliably identify where the spall has initiated, and the vibration levels within the bearing can be used to estimate the relative size of the spall so the appropriate spall prognostic models can be utilized.

In conclusion, the experimentally-observed spall growth patterns in bearing inner (cone) and outer (cup) rings, even under conditions of varying speed, load, and temperature suggest that a simple empirical model of spall area growth can be used as the basis for predicting safe residual useful life in a bearing when a spall is detected. If the developed spall area growth models are coupled with the bearing condition-monitoring algorithm that can detect the onset of spall formation, location, and estimated size, it can be used to schedule economical and proactive bearing replacement that minimizes unnecessary and costly train stoppages without reducing system reliability or increasing the risk of bearing failure and subsequent derailment.

ACKNOWLEDGMENT

The authors want to acknowledge the USDOT UTC program for making this study possible. The authors also want to thank Amsted Rail Industries engineers who provided many of the test bearings for this study.

FUNDING

This study was made possible by funding provided by The University Transportation Center for Railway Safety (UTCRS), through a USDOT Grant No. DTRT 13-G-UTC59.

DISCLOSURE STATEMENT

Any opinions, findings, conclusions or recommendations are those of the authors and do not necessarily reflect the views of the USDOT or Amsted Rail Industries.

REFERENCES

[1] SKF: Bearing designs, tapered roller bearing units. Extract from the Railway technical handbook, vol. 1, p. 76–87. [chapter 4].

[2] Tarawneh, C., Turner, J. A., Wilson, B. M., and Koester, L. (2013), "Service Life Testing of Railroad Bearings with Known Subsurface Inclusions Detected with Advanced Ultrasonic Technology," Int. J. of Railway Technology, **2**(3), pp 55-78.

[3] Sadeghi, F., Jalalahmadi, B., Slack, T. S., and Raje, N. K. (2009), "A Review of Rolling Contact Fatigue," ASME Journal of Tribology, **131**(4), 041403. DOI: 10.1115/1.3209132

[4] Tarawneh, C., Koester, L., Fuller, A. J., Wilson, B. M., and Turner, J. A. (2012), "Service Life Testing of Components with Defects in the Rolling Contact Fatigue Zone," ASTM International, STP 1548, West Conshohocken, PA, pp 67-83.

[5] Wilson, B. M., Fuller, A. J., Tarawneh, C., and Turner, J. A. (2016), "Near Race Inclusions in Bearing Components and the Resultant Effect on Fatigue Initiation and Component Life," *Proceedings of the Conference on Railway Excellence (CORE)*, Melbourne, Australia.

[6] Nikas, G. K. (2016), "Algebraic Equations for the Pile-Up Geometry in Debris Particle Indentation of Rolling Elastohydrodynamic Contacts," ASME Journal of Tribology, **138**(2), 021503. DOI: 10.1115/1.4031516

[7] Goshima, T., Ishihar, S., Shimizu, M., and Mizoguchi, A. (2010), "Crack Propagation and Initiation Lives for Surface Pitting Due to Rolling/Sliding Contact," Journal of Thermal Stresses, **33**(11), pp 1087-1106. DOI: 10.1080/01495739.2010.511917

[8] Gonzalez, A., Tarawneh, C., Wilson, B. M., and Turner, J. A. (2015), "Tracking of Spall Deterioration on Tapered Roller Bearing Raceways," *Proceedings of the ASME Joint Rail Conference*, San Jose, CA.

[9] Li, Y., Billington, S., Zhang, C., Kurfess, T., Danyluk, S., and Liang, S. (1999), "Dynamic Prognostic Prediction of Defect Propagation on Rolling Element Bearings," Tribology Transactions, **42**(2), pp 385-392.

[10] Qian, Y., Yan, R., and Gao, R. X. (2017), "A Multi-Time Scale Approach to Remaining Useful Life Prediction in Rolling Bearing," Mechanical Systems and Signal Processing, **83**, pp 549-567. https://doi.org/10.1016/j.ymssp.2016.06.031

[11] Zhou, Q., Xie, L., Jin, X., Wang, Z., Wang, J., Keer, L. M., and Wang, Q. (2014), "Numerical Modeling of Distributed Inhomogeneities and Their Effect on Rolling-Contact Fatigue Life," ASME Journal of Tribology, **137**(1), 011402. DOI: 10.1115/1.4028406

[12] Liu, H., Liu, H., Zhu, C., He, H., and Wei, P. (2018), "Evaluation of Contact Fatigue Life of a Wind Turbine Gear Pair Considering Residual Stress," ASME Journal of Tribology, **140**(4), 041102. DOI: 10.1115/1.4039164

[13] Association of American Railroads. *AAR Manual of Standards and Recommended Practices.* Section H "Journal Bearings and Lubrication" Specifications M-934. 2016. [Section 4.0 Design Criteria for AAR Class Bearings on page 61]

[14] Wilson, B. M., Fuller, A. J., Tarawneh, C., and Turner, J. A. (2015), "Early Bearing Fatigue Initiation by the Identification and Selection of Bearings with Near Race

Defects," *Proceedings of the International Heavy Haul Association Conference*, Perth, Australia.

[15] Tarawneh, C., Sotelo, L., De Los Santos, N., Villarreal, A., Lechtenberg, R., and Jones, R. (2016), "Temperature Profiles of Railroad Tapered Bearings with Defective Inner and Outer Rings," *Proceedings of the ASME Joint Rail Conference*, Columbia, SC.

[16] Montalvo, J., Tarawneh, C., and Fuentes, A. (2018), "Vibration-Based Defect Detection for Freight Railcar Tapered-Roller Bearings," *Proceedings of the ASME Joint Rail Conference*, Pittsburgh, PA.

[17] Tarawneh, C., Ley, J., Blackwell, D., Crown, S., and Wilson, B. M. (2018), "Onboard Load Sensor for Use in Freight Railcar Applications," Int. J. of Railway Technology, in press.

[18] De Los Santos, N., Jones, R., Tarawneh, C., and Villarreal, A. (2017), "Development of Prognostic Techniques for Surface Defect Growth in Railroad Bearing Rolling Elements," *Proceedings of the ASME Joint Rail Conference*, Philadelphia, PA.

[19] De Los Santos, N., Jones, R., Tarawneh, C., and Fuentes, A. (2018), "Defect Prognostic Models for Spall Growth in Railroad Bearing Rolling Elements," *Proceedings of the ASME Joint Rail Conference*, Pittsburgh, PA.

Table 1 Bearing cone (inner ring) and cup (outer ring) spall area growth rate values

	Spall Size	Average Growth Rate $[cm^2/km]\times10^{-4}$	Maximum Growth Rate $[cm^2/km]\times10^{-4}$	Minimum Growth Rate $[cm^2/km]\times10^{-4}$
Cone (Inner Ring)	< 6.45 cm^2 (1 in^2)	0.35	1.74	0.001
	> 6.45 cm^2 (1 in^2)	0.68	1.28	0.42
Cup (Outer Ring)	< 12.9 cm^2 (2 in^2)	1.01	3.83	0.07
	> 12.9 cm^2 (2 in^2)	3.41	6.52	1.09

Figure Captions List

Fig. 1	Typical railroad tapered-roller bearing assembly [1]
Fig. 2	Single bearing tester (SBT)
Fig. 3	Four-bearing dynamic test rig housed within an environmental chamber with a temperature range of -40°C to 60°C (-40°F to 140°F)
Fig. 4	Spall casting procedure; (left) spalled surface outlined with tacky tape; (right) Bismuth alloy cast into frame
Fig. 5	A series of pictures demonstrating the spall image processing and analysis to obtain the spall area. The "1" area in the figure is in square inches, while the other three measurements are in inches.
Fig. 6	Cone spall area versus total distance traveled since initiation
Fig. 7	Cone spall area growth ratio versus total distance traveled since initiation
Fig. 8	Cone spall growth pattern
Fig. 9	Cup spall growth pattern
Fig. 10	Cone spall area growth rate versus total distance traveled since initiation
Fig. 11	Cup spall area versus total distance traveled since initiation
Fig. 12	Projected area of a roller on the outer ring (cup) raceway
Fig. 13	Cup spall area growth ratio versus total distance traveled since initiation
Fig. 14	Cup spall area growth rate versus total distance traveled since initiation

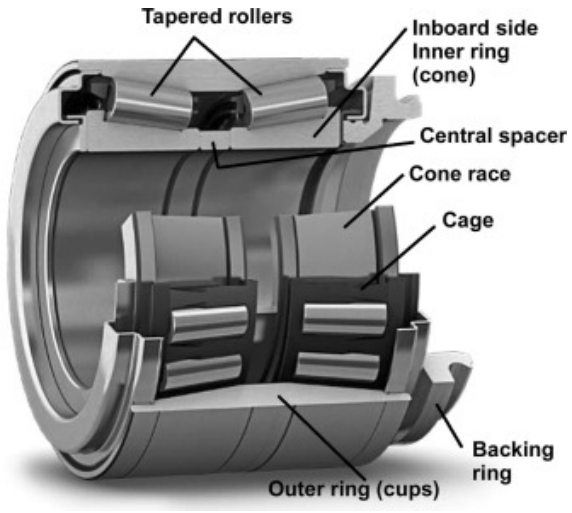

Fig. 1 Typical railroad tapered-roller bearing assembly [1]

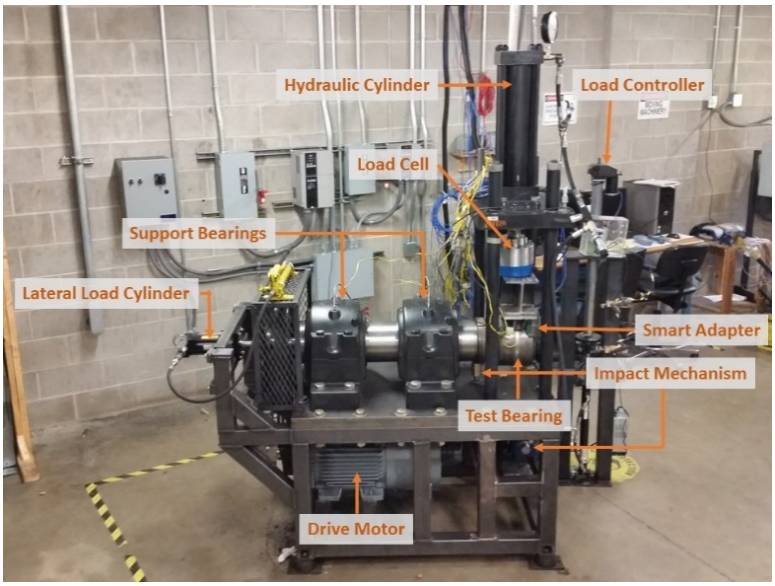

Fig. 2 Single bearing tester (SBT)

Fig. 3 Four-bearing dynamic test rig housed within an environmental with a temperature range of -40°C to 60°C (-40°F to 140°F)

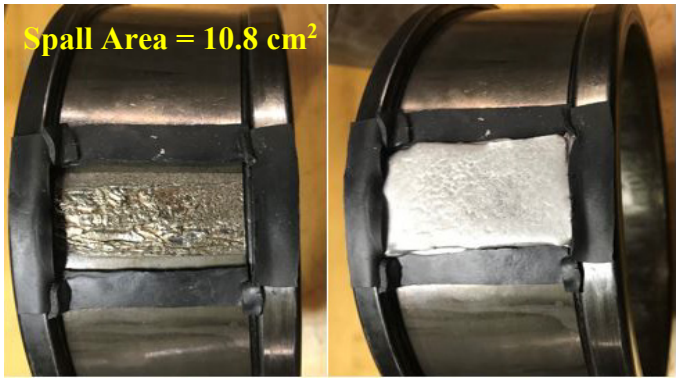

Fig. 4 Spall casting procedure; (left) spalled surface outlined with tacky tape; (right) Bismuth alloy cast into frame

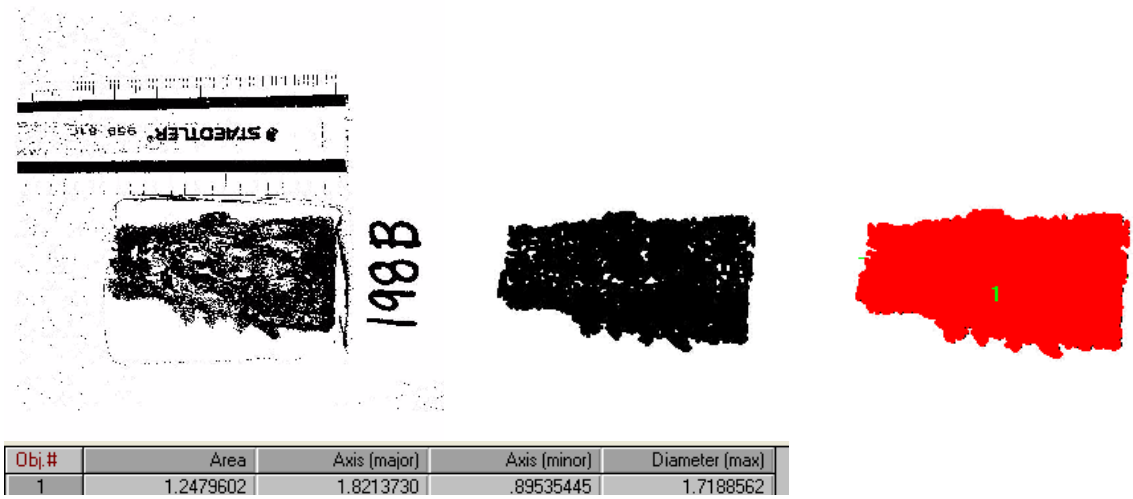

Obj.#	Area	Axis (major)	Axis (minor)	Diameter (max)
1	1.2479602	1.8213730	.89535445	1.7188562

Fig. 5 A series of pictures demonstrating the spall image processing and analysis to obtain the spall area. The “l” area in the figure is in square inches, while the other three measurements are in inches.

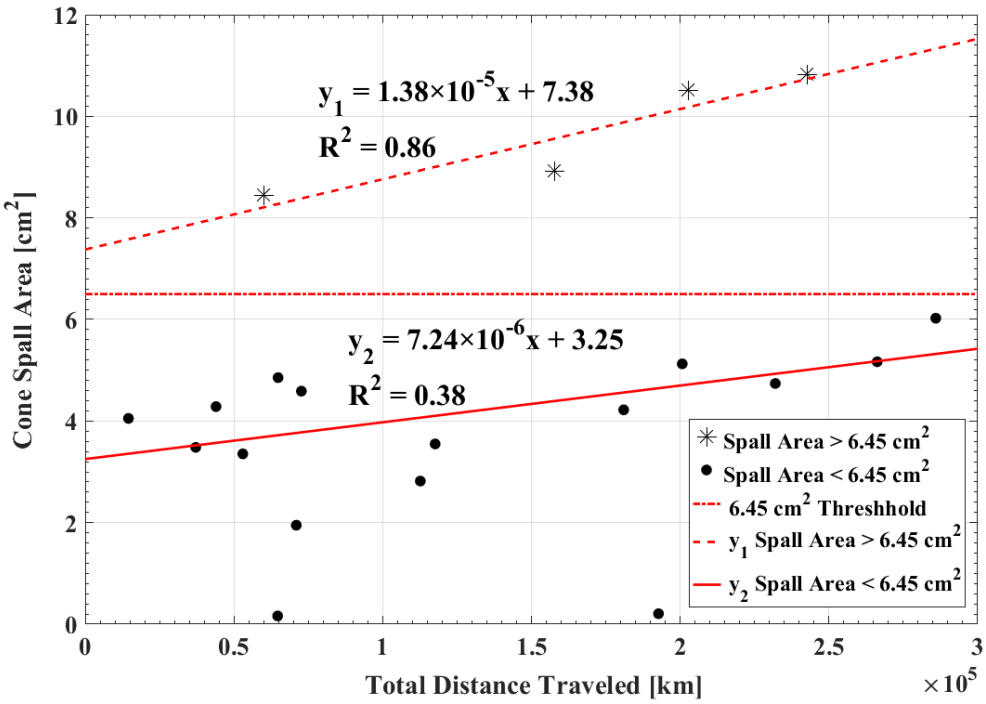

Fig. 6 Cone spall area versus total distance traveled since initiation

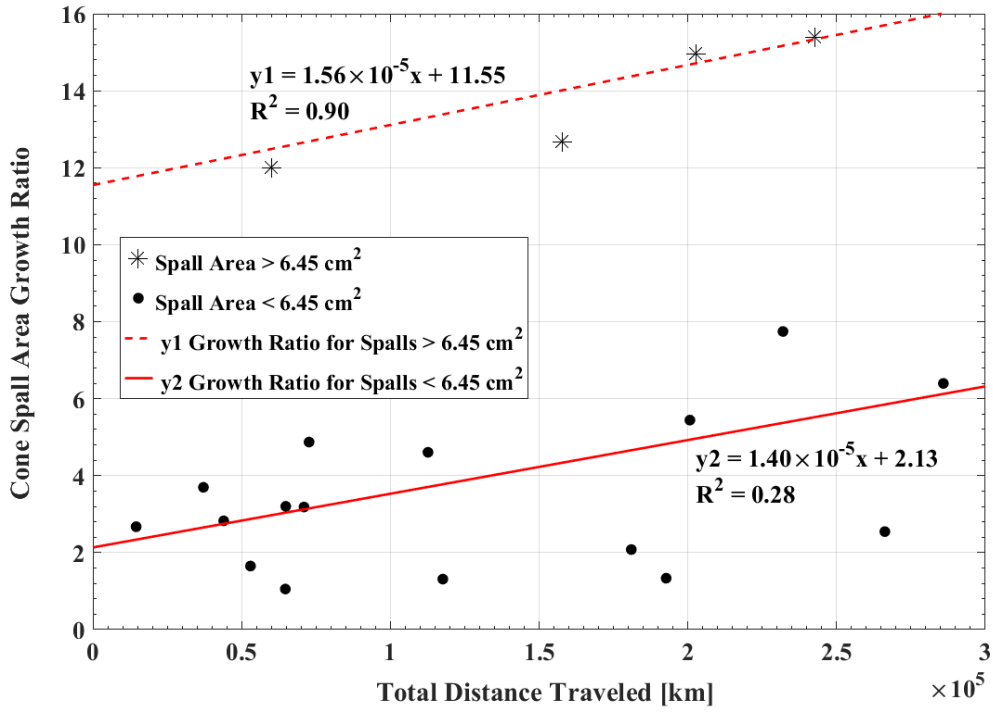

Fig. 7 Cone spall area growth ratio versus total distance traveled since initiation

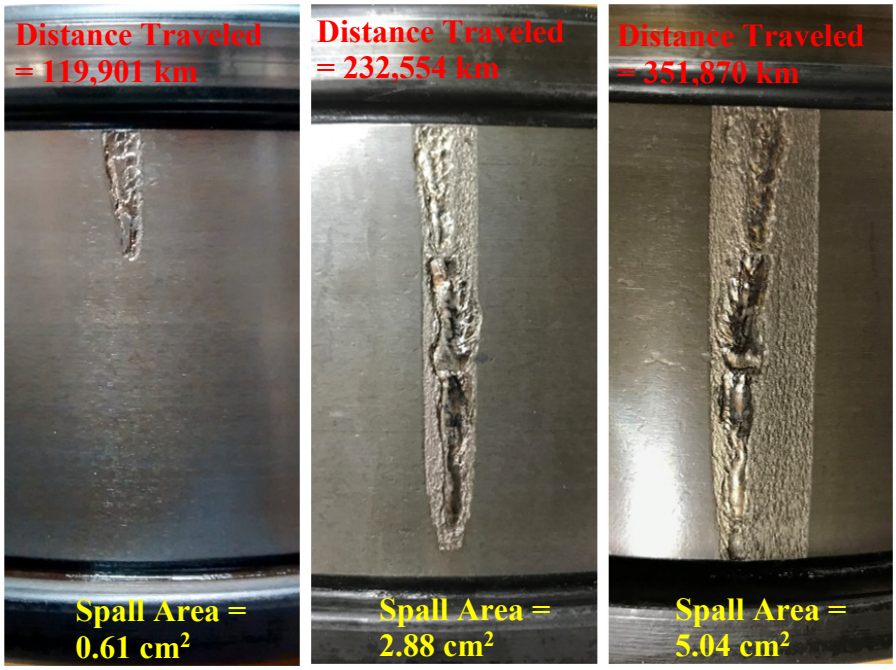

Fig. 8 Cone spall growth pattern

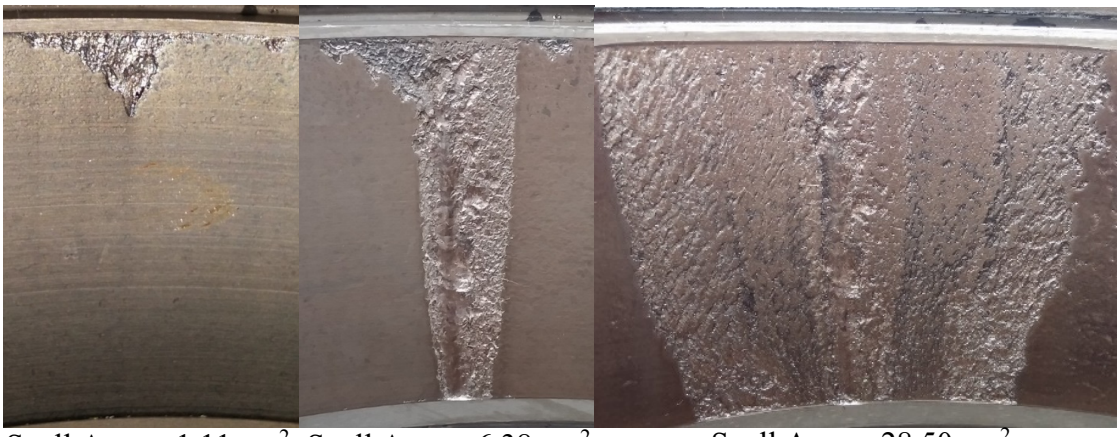

Spall Area = 1.11 cm^2
Distance Traveled = 82,750 km

Spall Area = 6.38 cm^2
Distance Traveled = 102,477 km

Spall Area = 28.50 cm^2
Distance Traveled = 124,731 km

Fig. 9 Cup spall growth pattern

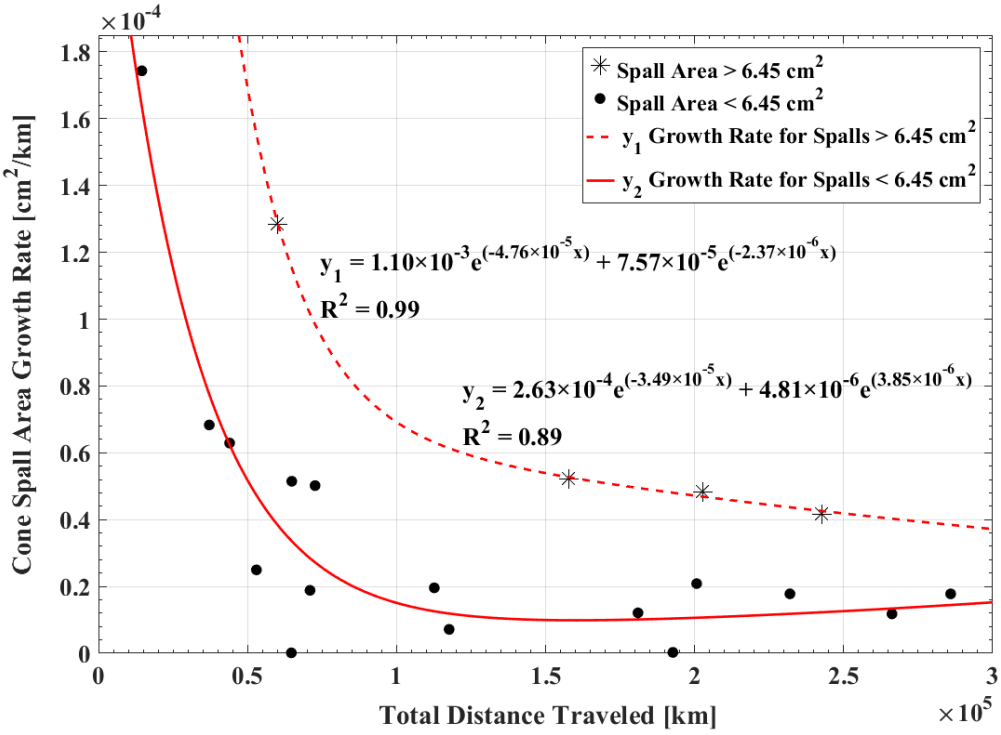

Fig. 10 Cone spall area growth rate versus total distance traveled since initiation

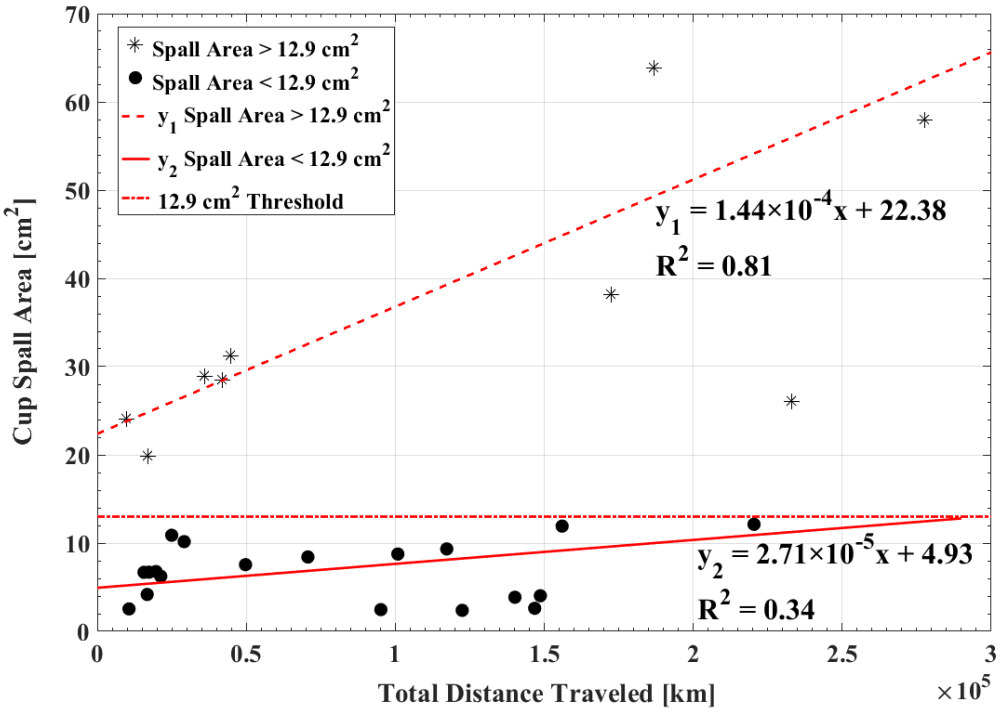

Fig. 11 Cup spall area versus total distance traveled since initiation

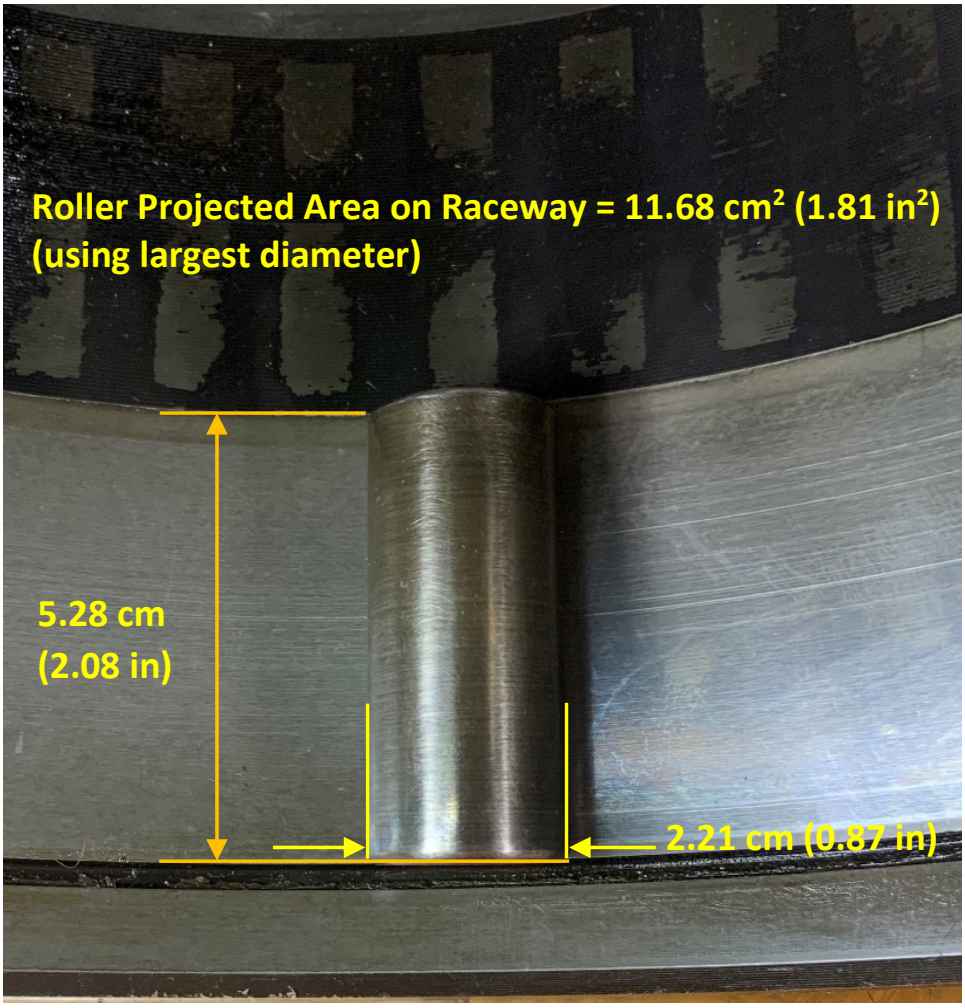

Fig. 12 Projected area of a roller on the outer ring (cup) raceway

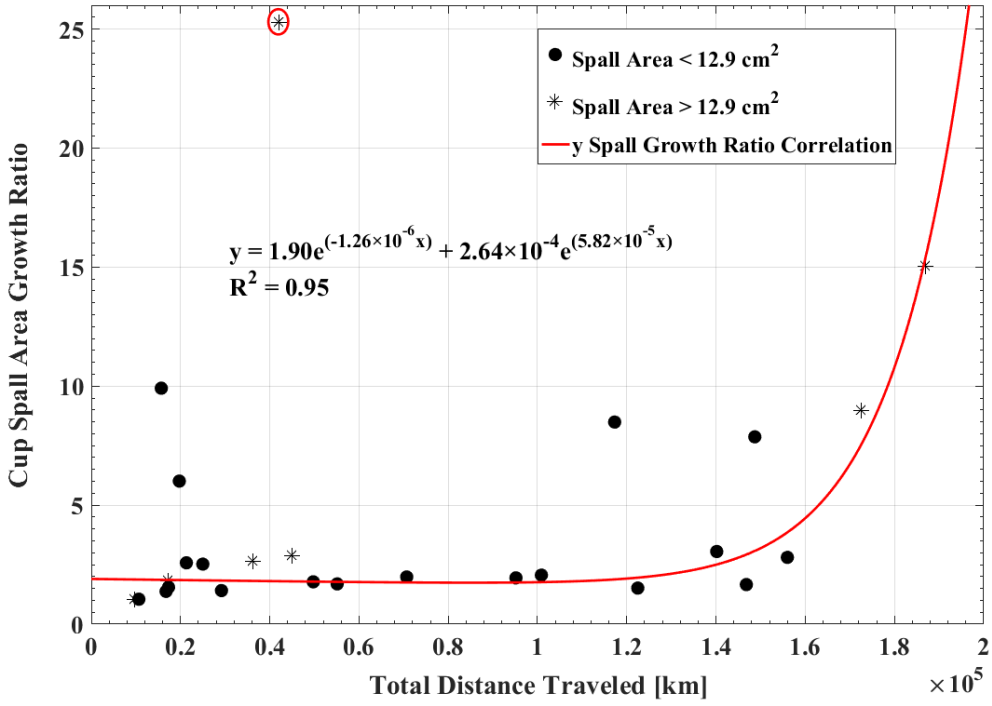

Fig. 13 Cup spall area growth ratio versus total distance traveled since initiation

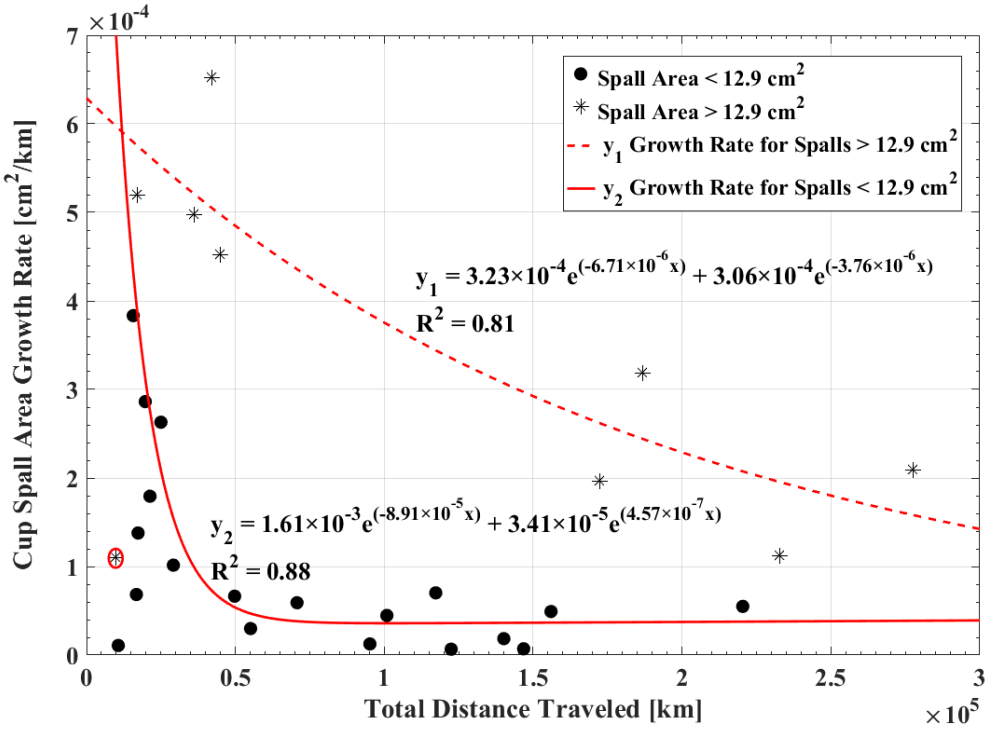

Fig. 14 Cup spall area growth rate versus total distance traveled since initiation